CHAPTER-3

Iron (III) ion-Facilitated Conversion of ZIF-67 to a Self-supported Fe_xCo-Layered Double Hydroxide for Improved Water Oxidation

In this chapter, Fe_xCo-layered double hydroxide (LDH) nanosheets has been used for achieving enhanced OER activity which was synthesized by the Lewis acid Fe(III)-assisted hydroxylation of ZIF-67. The best catalyst, $Fe_{0.4}Co$-LDH catalyst exhibited outstanding water oxidation activity, achieving a current density of 20 mA cm^{-2} at a mere 190 mV overpotential, outperforming hydrothermally synthesized LDH with a similar composition.

3.1. Introduction

Co-based LDHs have garnered significant attention for their potential in alkaline OER. However, their OER activity is limited due to the low free energy of *O binding on Co sites.[1][2][3][4] Additionally, the poor electronic conductivity of LDHs is a significant concern. The activity of Co-LDHs can be greatly enhanced by incorporating high-valence heterometal ions (such as Mo^{6+}, V^{5+}, Fe^{3+}, etc.) into their structure. Moreover, using self-supported catalysts on a conductive support can improve electronic conductivity and the catalyst-support interaction, leading to higher activity and stability.[5][6] Moreover, achieving an atomic-level thickness can further enhance the electrocatalytic activity of the LDH.[7]

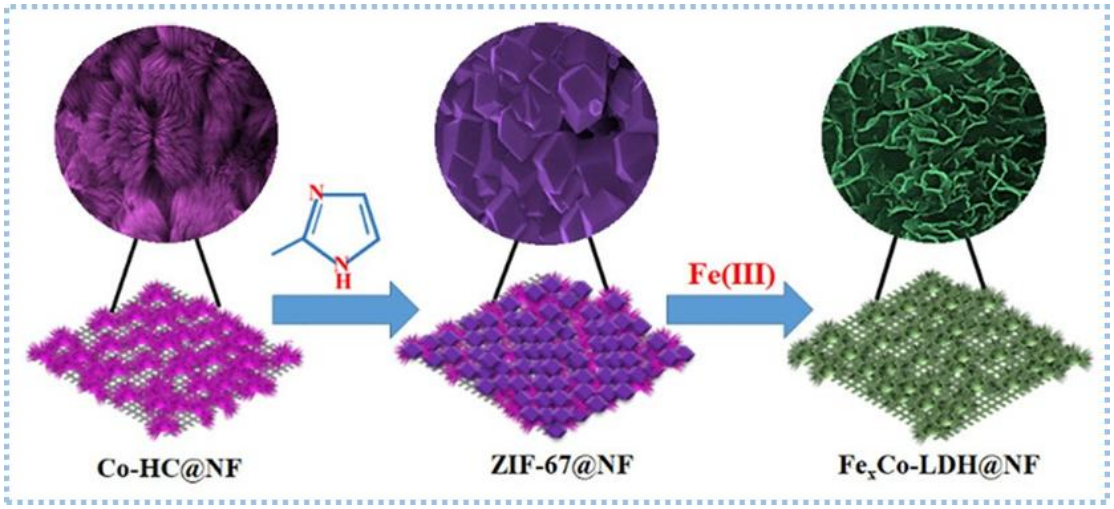

Scheme 3.1. Schematic diagram showing the synthesis of cobalt hydroxide carbonate (Co-HC) templated ZIF-67 on nickel foam, and its transformation into Fe_xCo-LDH by a Lewis acid Fe (III)-assisted hydroxylation method.

In this study, we have integrated the aforementioned factors to design self-supported Fe_xCo-LDH catalysts on nickel foam (NF). To accomplish this, we implemented a unique methodology, using self-supported Co-containing zeolitic imidazolate framework@NF (ZIF-67, a metal-organic framework, MOF) as the precursor for the synthesis of Fe_xCo-LDHs.[8] The Lewis acid Fe(III) facilitated the hydroxylation of ZIF-67, resulting in the formation of Fe_xCo-LDH nanosheets

(Scheme 3.1).[9] Simultaneously, the incorporation of Fe(III) into the Co-LDH structure markedly enhanced its water oxidation activity. Recently, our team and other research group have explored MOFs as precursors for LDHs, aiming to achieve superior electrochemical properties.

Treating ZIF-67 with Fe(III)-salt leads to the complete destruction of structure of the ZIF-67, yielding hierarchical nanosheets of FexCo-LDH@NF. In order to observe the impact of adding the strong Lewis acid Fe(III) to the structure of LDH we have prepared two more catalysts-Co-LDH [which were synthesized by the reaction of ZIF-67 with Co(II)] and ZnCo-LDH [synthesized by the reaction of ZIF-67 with Zn(II)]. Fe_xCo-LDHs exhibited significantly enhanced OER activity compared to Co-LDH and ZnCo-LDH due to the pronounced Lewis acid properties of Fe(III).

3.2. Chemicals

The acquisition of cobalt chloride hexahydrate was completed through Sigma Aldrich, with a purity level of 99.9%. The chemicals obtained from SRL, India include urea (99.5%), ammonium fluoride (98%), ferric nitrate nonahydrate, and 2-methyl imidazole. All chemicals were used without undergoing further purification. The purchase of nickel foam was sourced from AXYS technologies, an Indian company. Only double-distilled water was used for all the investigations and electrochemical tests.

3.3. Instruments

Instruments used for the characterization of the catalysts were same as mentioned in previous chapter except Scanning Probe Microscope (SPM) [NT-MDT Service & Logistics Ltd.] which was used for AFM characterization.

3.4. Experimental

3.4.1. Activation of nickel foam

Nickel foam was activated by the method mentioned in previous chapter**.**

3.4.2. Synthesis of cobalt hydroxide carbonate template on nickel foam (Co-HC@NF)

The precursor chemicals, including $CoCl_2.6H_2O$ (2 mmol), NH_4F (4 mmol), and urea (10 mmol), were dissolved in 12 mL of water. The reaction mixture was agitated at ambient temperature for a duration of 30 minutes and thereafter placed into a Teflon-lined autoclave with a volume of 50 mL. An activated nickel foam was vertically submerged in the solution, covering a geometrical area of 1 cm^2. The autoclave was tightly sealed and subjected to a temperature of 120 ^oC in an electric oven for a duration of 5 hours. Following the natural cooling of the cobalt hydroxide carbonate (Co-HC) coated nickel foam to room temperature, it was subsequently removed from autoclave and subjected to two rounds of rinsing with water and ethanol and after that dried at 60^oC for 12 h.[10]

3.4.3. Synthesis of iron cobalt hydroxide carbonate template on nickel foam ($Fe_{0.4}$Co-HC@NF)

$Fe(NO_3)_3 \cdot 9H_2O$ (0.4 mmol), $CoCl_2 \cdot 6H_2O$ (1.6 mmol), NH_4F (4 mmol), and urea (10 mmol) were dissolved in 12 mL of water. The resultant reaction mixture was stirred at ambient temperature for a duration of 30 minutes and thereafter transferred into a Teflon-lined autoclave with a volume of 50 mL. An activated nickel foam was vertically submerged in the solution, covering a geometrical area of 1 cm^2. The autoclave was tightly sealed and subjected to a temperature of 120 ^oC in an electric oven for a duration of 5 hours. Following the natural cooling of the cobalt hydroxide carbonate (Co-HC) coated nickel foam to room temperature, it was subsequently removed and subjected to two rounds of rinsing with water and ethanol and after that dried at 60^o C for 12 h.[10]

3.4.4. Synthesis of ZIF-67@NF

5 mmol of 2-methyl imidazole (2-MeIm) was dissolved in 5 mL of methanol in a 15 mL glass container. Next, the Co-HC@NF was dipped in a vertical position in the solution of 2-MeIm that

had been prepared. The vial was sealed and stored at an ambient temperature for a duration of 12 hours. After this duration, a purple-colored ZIF-67 was found, which indicated the conversion of Co-HC@NF into ZIF@NF. The ZIF-67@NF obtained was subjected to multiple washes with methanol to eliminate any remaining 2-MeIm, and then dried at 60°C for a duration of 12 hours.[11]

3.4.5. Synthesis of $Fe_{0.4}$Co-ZIF-67@NF

5 mmol of 2-methyl imidazole (2-MeIm) was dissolved in 5 mL of methanol in a glass vial with the volume. After that, $Fe_{0.4}$Co-HC@NF was immersed vertically in the as prepared 2-MeIm solution. Subsequently vial was sealed and left at room temperature for 12 hours. After this period, $Fe_{0.4}$CoZIF-@NF deposited on NF was obtained. The resulting $Fe_{0.4}$CoZIF-@NF was washed multiple times with methanol to remove any residual 2-MeIm and subsequently dried at 60°C for 12 hours.[11]

3.4.6. Synthesis of $Fe_{0.4}$ Co-LDH@NF

0.04 mmol of $Fe(NO_3)_3 \cdot 9H_2O$ was dissolved in a mixed solution of isopropanol and ethylene glycol (8:2). The solution was then transferred into a Teflon-lined autoclave. The as-synthesized ZIF@NF was dipped into the reaction mixture in vertical manner and then autoclave was sealed. Subsequently, the sealed autoclave was heated at 120°C in an electric oven for 5 hours. Afterward, the reaction mixture was allowed to cool down to room temperature. $Fe_{0.4}$Co-LDH@NF was then dried at 60°C overnight.[12]

3.4.7. Synthesis of Co-LDH@NF

Co-LDH@NF was synthesized following the same procedure used $Fe_{0.4}$Co-LDH@NF, but 0.04 mmol of $Fe(NO_3)_3 \cdot 9H_2O$ was replaced by $Co(NO_3)_2 \cdot 6H_2O$.[12]

3.4.8. Synthesis of ZnCo-LDH@NF

ZnCo-LDH@NF was prepared following the same method as $Fe_{0.4}$Co-LDH@NF, but with

$Fe(NO_3)_3 \cdot 9H_2O$ replaced by 0.04 mmol of $Zn(NO_3)_2 \cdot 6H_2O$.[12]

3.5. Results and discussion

3.5.1. Characterizations of the catalysts

A reaction was performed between nickel foam supported cobalt (II) hydroxide carbonate and 2-methyl imidazole in order to produce the catalyst precursor ZIF-67@NF **(Scheme 3.1)**. ZIF-67@NF exhibited the characteristic crystal planes of ZIF-67, as demonstrated by the powder X-ray diffraction (PXRD) pattern (JCPDS: 08-60-513, **Figure 3.1a**). The Lewis acid Fe (III) catalyzed the hydroxylation of ZIF-67 to form Fe_xCo-LDH nanosheets **(Scheme 3.1)**. In addition, Fe (III) was introduced in the structure of Co-LDH during the transformation and significantly improved the water oxidation activity. Recently, we and other groups also explored MOFs as the precursors of LDHs to achieve exceptional electrochemical properties The treatment with Fe (III)-salt results in the complete destruction of the structure of ZIF-67 and produces hierarchical nanosheets of Fe_xCo-LDH@NF. The powder X-ray diffraction (PXRD) pattern indicated that $Fe_{0.4}Co$-LDH@NF exhibits a rhombohedral phase of Co-LDH with a space group of R_{3m} **(Figure 3.1a)**.[13] Comparing $Fe_{0.4}Co$-LDH@NF with Co-LDH@NF revealed a peak shift of 0.26 (2 theta degrees) due to the incorporation of Fe (III) into Co-LDH. The interlayer d-spacing of 7.67 Å corresponding to the (003) plane indicates the presence of CO_3^{2-} as the anion between the metal hydroxide layers.[14] Additionally, the Fourier Transformed Infrared (FTIR) spectrum exhibited a distinct peak at 1375 cm^{-1}, which confirmed the presence of CO_3^{2-} anions (**Figure 3.1b**).[15]

X-ray photoelectron spectroscopy (XPS) was employed to investigate how the incorporation of Fe affects the surface and electronic structure of the catalysts **(Figure 3.1c)**. The peaks observed at 783.1 eV (Co $2p_{3/2}$) and 797.39 eV (Co $2p_{1/2}$) were assigned to Co^{2+}, while those at 779.68 eV and 795.47 eV were attributed to Co^{3+} in the X-ray photoelectron spectroscopy (XPS) analysis.[16]

Table 3.1. Details of all synthesized Fe_xCo-LDH catalysts.

Catalyst	Precursor	Amount of salt
Co-LDH@NF	ZIF-67@NF	$CoCl_2.6H_2O$ (0.4 mmol)
ZnCo-LDH@NF	ZIF-67@NF	$Zn(NO_3)_2.6H_2O$ (0.4 mmol)
$Fe_{0.1}$Co-LDH@NF	ZIF-67@NF	$Fe(NO_3)_3.9H_2O$ (0.1 mmol)
$Fe_{0.2}$Co-LDH@NF	ZIF-67@NF	$Fe(NO_3)_3.9H_2O$ (0.2 mmol)
$Fe_{0.3}$Co-LDH@NF	ZIF-67@NF	$Fe(NO_3)_3.9H_2O$ (0.3 mmol)
$Fe_{0.4}$Co-LDH@NF	ZIF-67@NF	$Fe(NO_3)_3.9H_2O$ (0.4 mmol)
$Fe_{0.5}$Co-LDH@NF	ZIF-67@NF	$Fe(NO_3)_3.9H_2O$ (0.5mmol)

In $Fe_{0.4}$Co-LDH, the Co $2p_{3/2}$ peak exhibited a positive shift of 0.6 eV relative to that of Co-LDH, suggesting an enhancement in the positive charge density on the Co atom due to the incorporation of Fe into the catalyst structure. Additionally, the spin-orbit coupling spacing value between Co $2p_{3/2}$ and Co $2p_{1/2}$ decreased from 15.83 eV (in Co-LDH) to 15.32 eV in $Fe_{0.4}$Co-LDH. This result indicates a higher concentration of Co^{3+} in $Fe_{0.4}$Co-LDH@NF compared to Co-LDH@NF. The Fe 2p spectra displayed two primary peaks, one at 710.21 eV and the other at 723.75 eV corresponding to Fe $2p_{3/2}$ and Fe $2p_{1/2}$ respectively. The spin-orbit coupling value of 13.37 eV for Fe $2p_{3/2}$-Fe$2p_{1/2}$ indicated that Fe(III) is the predominant species **(Figure 3.1d)**.[13] As a result of the electron density being transferred from Co(II) to Fe(III), the Fe 2p spectra of $Fe_{0.4}$Co-LDH was found to be negatively shifted in comparison to that of Fe_2O_3 [17] indicating decrease in positive charge on Fe .

Therefore, the X-ray photoelectron spectroscopy (XPS) results for both Co 2p and Fe 2p in

$Fe_{0.4}$Co-LDH@NF confirm the electronic interaction between these two metal centres, leading to a redistribution of charge between Co(II) and Fe(III).

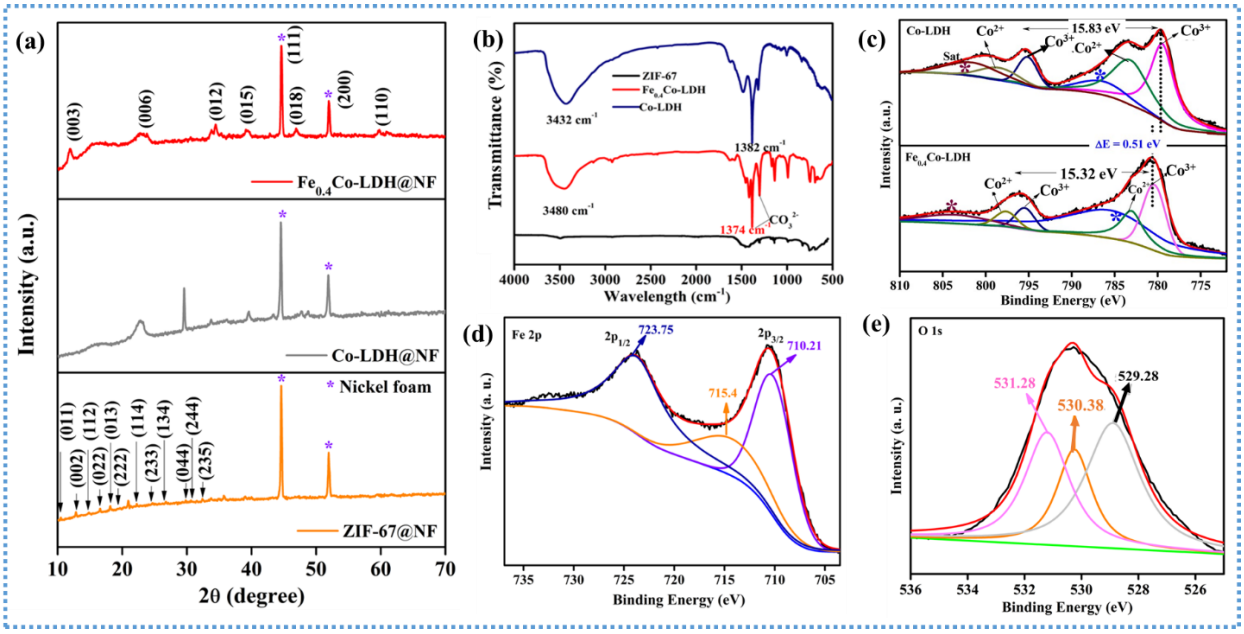

Figure 3.1. (a) The PXRD graph of ZIF-67@NF, Co-LDH@NF and $Fe_{0.4}$Co-LDH@NF; (b) shows the FTIR spectra of ZIF-67@NF, Co-LDH@NF and $Fe_{0.4}$Co-LDH@NF; (c) The Co 2p XPS spectra of Co-LDH and $Fe_{0.4}$Co-LDH showing the modulation of the electronic structure after the introduction of Fe(III) in the structure of the catalyst. The * marked peaks are satellite peaks of Co(II); (d) Fe 2p X-ray photoelectron spectrum of $Fe_{0.4}$Co-LDH. The Fe2p spectrum was deconvoluted into two peaks with binding energy 724.15 eV and 710.61 eV corresponding to Fe $2p_{1/2}$ and Fe $2p_{3/2}$ (e) The O 1s XPS was fitted into three peaks for the oxygen of water (531.28 eV), surface oxygen (530.38 eV), and Co/Fe-O bond (529.38 eV).

The O 1s XPS spectrum was deconvoluted into three peaks representing oxygen from water (531.28 eV), surface oxygen (530.38 eV), and the Co/Fe-O bond (529.38 eV) **(Figure 3.1e)**. [16] Scanning electron microscopy (SEM) images revealed uniform growth of ultrathin nanosheets of $Fe_{0.4}$Co-LDH on the surface of the nickel foam **(Figure 3.2a)**.

It has also been demonstrated by scanning electron microscopy (SEM) that the dodecahedron morphology of ZIF-67@NF was completely destroyed after being treated with Lewis acid Fe (III)

(Figure 3.2a inset). Transmission electron microscopy (TEM) images showed the presence of 2D ultrathin nanosheets comprising $Fe_{0.4}$Co-LDH **(Figure 3.2 f-g)**. The thickness of the vertically oriented nanosheets was determined to be approximately 4 nm **(Figure 3.2f-g)**.

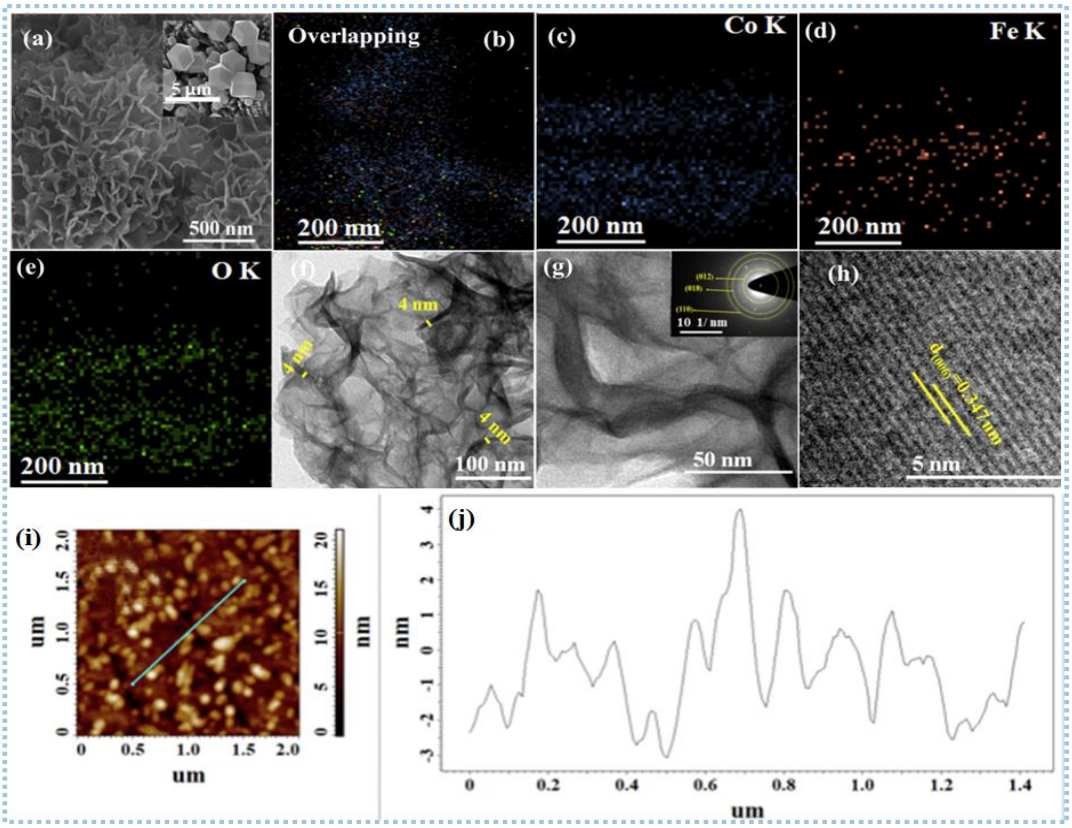

Figure 3.2. (a) SEM image showing the uniformly grown nanosheets of $Fe_{0.4}$Co-LDH@NF on nickel foam (inset ZIF-67); (b-e) Corresponding elemental mapping showing the uniform distribution of all the element; (f)TEM image showing the nanosheets of $Fe_{0.4}$Co-LDH having an atomic level thickness; (g) TEM image showing the transparent nanosheets of $Fe_{0.4}$Co-LDH, inset SAED pattern of $Fe_{0.4}$Co-LDH; (h) HR-TEM image showing the d-spacing of 0.347, corresponding to the (006) plane of $Fe_{0.4}$Co-LDH; (i) AFM image of $Fe_{0.4}$Co-LDH@NF and (j) corresponding height profile showing the ~ 4 nm thickness of the nanosheets. The thin nanosheets offer a large number of active sites with coordinative and electronic unsaturation for substrate binding as well as high active surface area.

Additionally, atomic force microscopy (AFM) was used to measure the thickness of $Fe_{0.4}$Co-LDH nanosheets, which was found to be approximately 4 nm **(Figure 3.2i-j)**. In order to gain access to

a large number of active sites for the electrochemical water oxidation, the thickness of the nanosheets at the atomic level is of the utmost importance. In addition, the coordinative and electronic unsaturation that occurs in ultrathin nanosheets makes it easier for the substrate to bind to the surface of the catalyst, which in turn improves the catalytic activity.

(HR-TEM) analysis of $Fe_{0.4}$Co-LDH revealed a d-spacing of 0.347 nm, which corresponds to the (006) plane of Co-LDH **(Figure 3.2h)**.[13] For the confirmation of the presence of the elements Fe, Co, O, and C in $Fe_{0.4}$Co-LDH, energy dispersive X-ray spectroscopy (EDX) was performed and elemental mapping demonstrated that all elements were distributed in a uniform manner **(Figure 3.2b-e)**. The selected area electron diffraction (SAED) pattern of $Fe_{0.4}$Co-LDH displayed three rings which can be correlated to the crystal planes of Co-LDH, which are (018), (012), and (113) **(Figure 3.2g inset)**.

3.5.2. Electrochemical Activity

The electrocatalytic performance of $Fe_{0.4}$Co-LDH@NF and other synthesized catalysts was assessed using a three-electrode setup with a scan rate of 5 mV s^{-1} in a 1.0 M aqueous KOH solution. The linear sweep voltammetric (LSV) polarization curves demonstrated that $Fe_{0.4}$Co-LDH@NF exhibited the best OER activity among the synthesized catalysts **(Figure 3.3a)**. The introduction of Fe(III) into Co-LDH structure has a significant impact, resulting in all the Fe_xCo-LDH@NF catalysts exhibiting superior OER activity compared to both Co-LDH and ZnCo-LDH **(Figure 3.3b)**. Furthermore, varying the amount of Fe(III) in Fe_xCo-LDH@NF significantly impacts the OER activity, with the overpotential ranging widely from 240 mV to 370 mV at a current density of 100 mA cm^{-2} **(Figure 3.3d-e)**. The overpotential for the OER decreased as the amount of Fe(III) in Co-LDH increased, reached an optimal value for $Fe_{0.4}$Co-LDH@NF, and then increased with further Fe(III) addition **(Figure 3.3e)**.

Interestingly, $Fe_{0.4}$Co-LDH@NF achieved a current density of 20 mA cm^{-2} with an overpotential of just 190 mV, which is significantly lower than the 365 mV, required by Co-LDH. $Fe_{0.4}$Co-LDH@NF achieved a current density of 100 mA cm^{-2} with an overpotential as low as 240 mV. Furthermore, $Fe_{0.4}$Co-LDH@NF exhibits superior OER activity compared to $Fe_{0.4}$Co-ZIF@NF and ZIF-67@NF **(Figure 3.3a)**. $Fe_{0.4}$Co-LDH@NF demonstrated superior OER activity compared to $Fe_{0.4}$Co-HC@NF, which was prepared via the hydrothermal method **(Figure 3.3a)**.

These findings clearly illustrate the distinctive electrochemical characteristics of $Fe_{0.4}$Co-LDH@NF, originating from ZIF-67 through the robust Lewis acid Fe(III)-assisted hydroxylation process. Certainly, the overpotential achieved by $Fe_{0.4}$Co-LDH@NF for the OER surpasses that of cobalt-based LDHs reported in the literature as well as catalysts derived from ZIF-67 **(Table 3.2 and 3.3)**.

The kinetics of the OER with the synthesized catalysts were evaluated using Tafel analysis under semi-stationary conditions **(Figure 3.3c-d)**. $Fe_{0.4}$Co-LDH@NF exhibited the lowest Tafel slope (53 mV dec^{-1}), confirming its superior OER kinetics. Additionally, in the comparative analysis of the catalysts' Tafel slopes, $Fe_{0.4}$Co-LDH@NF showed the lowest Tafel slope among all the Fe_xCo-LDHs@NF investigated.

To elucidate the superior water oxidation activity of $Fe_{0.4}$Co-LDH@NF compared to other catalysts, we conducted an in-depth study of the electrochemical properties of these catalysts. The cyclic voltammetry (CV) of $Fe_{0.4}$Co-LDH@NF two redox peaks were observed corresponding to the oxidation of Co(II) to Co(III) at 1.13 V vs RHE and Co(III) to Co(IV) at 1.35 V vs RHE respectively **(Figure 3.3f)**.[16] In the CV of Co-LDH@NF, a peak was observed at a higher potential (1.39 V vs RHE) compared to that in $Fe_{0.4}$Co-LDH@NF.

The presence of Fe(III) ions in $Fe_{0.4}$Co-LDH@NF facilitates the electron density withdrawal from

Co(II), thereby promoting the oxidation of Co(II) to Co(III) and subsequently to Co(IV).

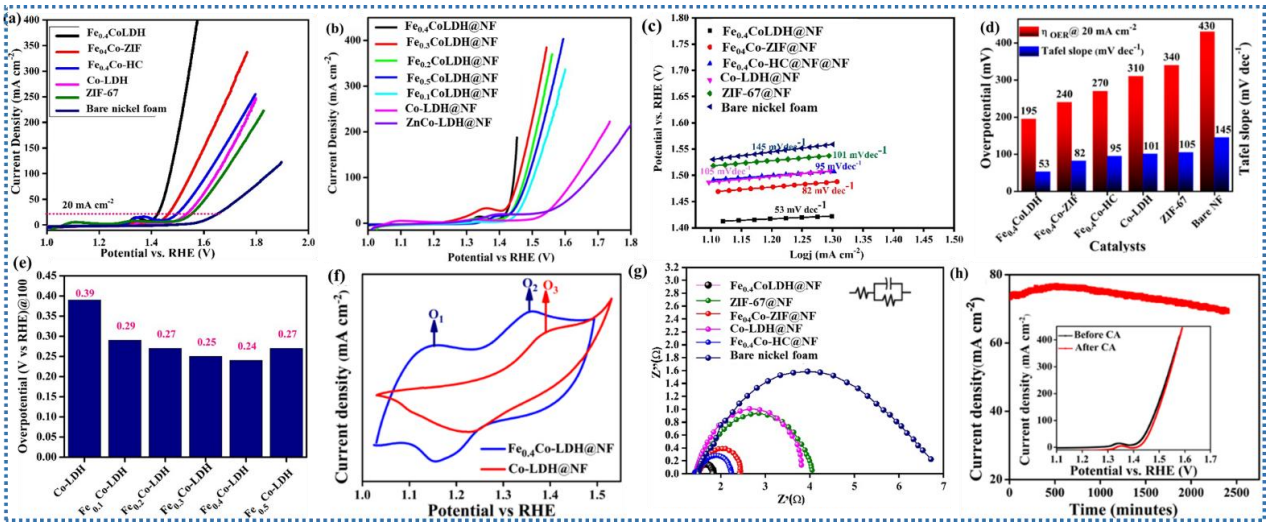

Figure 3.3. (a, b) LSV profiles for OER of Fe_xCo-LDH@NF catalysts having different amount of Fe(III) in the structure**;** (c) Tafel plots of all synthesized catalysts for OER; (d) comparative plots of the overpotentials and Tafel slopes for the catalysts showing the best activity and fastest kinetics for $Fe_{0.4}Co$-LDH@NF; (e) Comparison of the overpotential of the catalysts to reach a current density of 100 mA cm^{-2} ; (f) CV profiles of $Fe_{0.4}Co$-LDH@NF and Co-LDH showing the redox peaks for the oxidation of Co^{II} to Co^{III} and Co^{III} to Co^{IV} during the OER; (g) demonstrates Nyquist plots for the $Fe_{0.4}Co$-LDH@NF, Co-LDH@NF, ZIF-67@NF, $Fe_{0.4}Co$-ZIF@NF, $Fe_{0.4}Co$-HC@NF, and bare nickel foam obtained from electrochemical impedance spectroscopic (EIS) measurements showing lowest charge transfer resistance for $Fe_{0.4}Co$-LDH@NF. The spectra were collected with an anodic polarization potential of 1.48 V vs RHE**;** (h) chronoamperometric stability test of $Fe_{0.4}Co$-LDH@NF and inset showing negligible change in the LSV profile after a 40 h long high current density chronoamperometric study.

The easy formation of Co^{IV} = O species in $Fe_{0.4}Co$-LDH@NF facilitates the attack of nucleophilic OH- ions, promoting the formation of O-O bonds.[30] Because Fe^{III} has three unpaired electrons which occupy t_{2g} orbitals, therefore, incorporation of Fe^{III} in the catalyst structure establishes robust electronic interaction with Co^{II} and Co^{III}. Consequently, electron density from the t_{2g} orbitals of Co^{II} and Co^{III} is partially transferred to the t_{2g} orbitals of Fe^{III}, involving bridging O^{2-}. This process aids in stabilizing the Co centre in its higher oxidation states such as 3+ and 4+,

thereby enhancing the water oxidation activity.[31]

Table 3.2. The OER activities of reported LDHs compared with $Fe_{0.4}$Co-LDH@NF.

Sr. No.	Catalyst	Current density (mA cm^{-2})	Overpotential (mV)	Reference
1	**$Fe_{0.4}$Co-LDH@NF**	**20**	**190**	**This work**
2	CoFe-LDH-Ar@NF	10	299	[18]
3	NiCoFe-LDH@CFP	10	239	[19]
4	NiCo-LDH nanoplates@CP	10	367	[20]
5	CoMoV-LDHs@NF	10	270	[21]
6	CoFe-LDH@Cu NWs	10	240	[22]
7	H_2O-plasma CoFe-LDH	10	232	[23]
8	NiCoFe-LDHs/CFC	10	239	[19]
9	$Ni_{76}Co_{24}$-LDHs@NF	10	293	[24]
10	CoNiP/NiFe-LDH	10	210	[24]
11	$Ni_3Co_3Fe_3$-LDH	10	290	[25]
12	E-CoFe-LDHs	10	300	[26]
13	ZnFeCo-LDH	10	221	[27]
14	CoMn-LDH nanosheets	10	324	[28]
15	NiCo-LDH nanosheets	10	299	[29]

Additionally, electrochemical characterizations such as electrochemical impedance spectroscopy (EIS) and double-layer capacitance also demonstrate the superior performance of $Fe_{0.4}$Co-LDH compared to Co-LDH. The impedance spectra revealed that the addition of Fe(III) into Co-LDH notably decreased the charge transfer resistance (R_{ct}) **(Figure 3.3g)**. The R_{ct} value of 0.42 Ω observed for $Fe_{0.4}$Co-LDH indicates that it demonstrates the fastest charge transfer kinetics among the catalysts.

The electrochemical active surface area (ECSA) of the catalysts can be assessed through electric double-layer capacitance (C_{dl}) measurements in the non-faradaic region **(Figure 3.4)**. $Fe_{0.4}$Co-LDH@NF exhibits the highest C_{dl} value among the catalysts, indicating the highest ECSA **(Figure**

3.5 a and table 3.4).

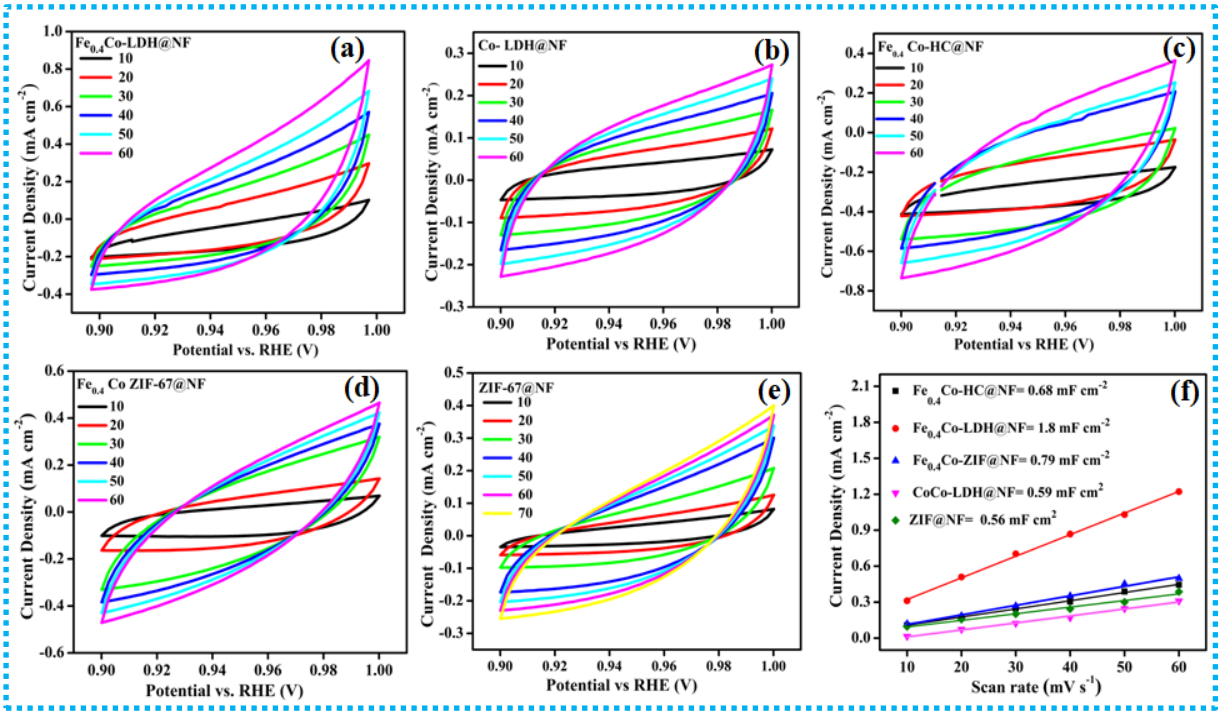

Figure 3.4. Determination of double-layer capacitance (C_{dl}) of $Fe_{0.4}$Co-LDH, Co-LDH@NF, $Fe_{0.4}$Co-HC@NF, $Fe_{0.4}$Co-ZIF@NF and ZIF-67@NF by plotting (difference in current density)/2 against scan rate.

The normalized OER activities based on ECSA also confirmed that $Fe_{0.4}$Co-LDH exhibits the best performance among the catalysts **(Figure 3.5b)**. A similar pattern was also noted for the number of active sites in the LDHs (**(Figure 3.5 d and table 3.5)**. $Fe_{0.4}$Co-LDH@NF was found to have the highest number of active sites (97.3×10^{14}) among the synthesized catalysts **(Figure 3.5d and equation 3.1)**.

The number of active sites almost linearly increased with the increase of the ECSA from Co-LDH to $Fe_{0.3}$Co-LDH, attained the highest value for $Fe_{0.4}$Co-LDH and dropped suddenly for $Fe_{0.5}$Co-LDH **(Figure 3.5e)**.

The ECSA of a catalyst is calculated from the double layer capacitance according to the formula:

$$ECSA = C_{dl}/C_s \quad (5)$$

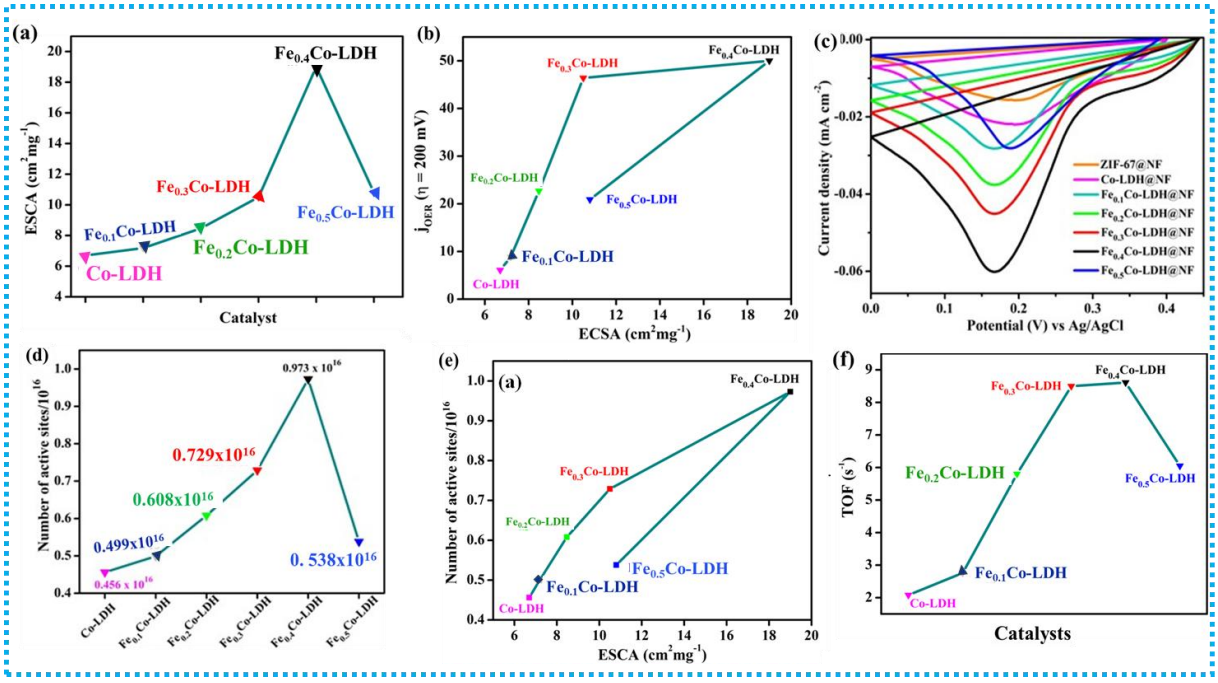

Figure 3.5. (a) Plot of ECSA vs Catalyst Fe_xCo-LDHs@NF. The plot shows that the ECSA is increased up to $Fe_{0.4}$Co-LDH with increase in the iron substitution after that no increment in ECSA is observed; (b) The OER current density of different catalysts attained at 200 mV overpotential plotted against ECSA; (c) Potential vs current density plots showing the reduction peak used for the area integration curve; (d) The number of active sites of Fe_xCo-LDH@NF having different amount of Fe(III); (e) Plot of the number of active sites vs ECSA for Fe_xCo-LDHs@NF; (f) Plot for the turn over frequency (TOF) of catalysts Fe_xCo-LDHs@NF.

Where C_{dl} is double layer capacitance of the catalyst and C_s is specific capacitance of the material per unit area under identical electrolyte conditions. Cs = 0.040 mF cm^{-2} in 1.0 M KOH based on reported values.[44] For a better understanding of the intrinsic OER activity, the turnover frequencies (TOFs) of the catalysts were calculated by equation given below-

For $Fe_{0.4}$Co-LDH, Calculated area associated with the reduction peak = 7.79 x 10^{-6} V A Hence the

associated charge is = 7.799 x 10^{-6} V A / 0.005 V s^{-1}

= 1.559 x 10^{-3} A s

= 1.559 x 10^{-3} C

Table 3.3. The determination of C_{dl} and ECSA of Fe_xCo-LDH.

Sr. No.	Catalyst	C_{dl} (mF cm^{-2})	ECSA (cm^2 mg^{-1})
1	Co-LDH	0.59	6.70
2	$Fe_{0.1}$Co-LDH	0.69	7.18
3	$Fe_{0.2}$Co-LDH	0.78	8.47
4	$Fe_{0.3}$Co-LDH	1.01	10.50
5	$Fe_{0.4}$Co-LDH	1.8	19.00
6	$Fe_{0.5}$Co-LDH	1.02	10.80

Equation 3.1: Determination of surface active sites using area integration of reduction peak [45][46]

Now, the number of electron transferred is = 1.559 x 10^{-3} C / 1.602 ×10^{-19} C

= 0.973 x 10^{16}

Since the reduction of Co^{3+} to Co^{2+} is a single electron transfer reaction, the number of electrons calculated above is the same as the number of surface-active sites.

Hence,

The surface-active site that participated in OER is = 0.973 x 10^{16}

Equation 3.2: Calculation of Turn over frequency (TOF) of different catalyst.[45][46]

$$TOF = (j \times NA) / (4 \times F \times n) \quad (7)$$

Where,

j = current density at η = 200 mV NA = Avogadro number

F = Faraday constant

n = number of active Co-sites

For $Fe_{0.4}$Co-LDH

TOF = [(50 x 10^{-3}) x (6.023 x 102^{3})] / [(4) x (96485) x (0.973 x 10^{16})]

= 8.61 s^{-1}

The turnover frequency (TOF) increased gradually with an increasing amount of Fe(III) in the catalyst structures, peaked at $Fe_{0.4}$Co-LDH@NF (TOF = 8.61 s^{-1}), and declined with further increases in Fe(III) content **(Figure 3.5f)**.

Table 3.4. Area under the curve, no. of active site and turnover frequency of Fe_xCo-LDH catalysts.

Sr. No.	Catalyst	Area under the curve (VA)	No. of active site (n)	TOF (s^{-1})
1	Co-LDH	3.656 x 10^{-6}	0.456 x 10^{16}	2.08
2	$Fe_{0.1}$Co-LDH	3.997 x 10^{-6}	0.499 x 10^{16}	2.76
3	$Fe_{0.2}$Co-LDH	4.874 x 10^{-6}	0.608 x 10^{16}	5.80
4	$Fe_{0.3}$Co-LDH	5.849 x 10^{-6}	0.729 x 10^{16}	8.50
5	$Fe_{0.4}$Co-LDH	7.799 x 10^{-6}	0.973 x 10^{16}	8.61
6	$Fe_{0.5}$Co-LDH	4.310 x 10^{-6}	0.538 x 10^{16}	6.00

Therefore, achieving an optimal concentration of Fe(III) in Co-LDH is essential to maximize the activity of Fe_xCo-LDH@NF and enhance the superior OER activity of Fe_xCo-LDHs over Co-

LDH. Moreover, the practical application of an electrocatalyst heavily relies on its durability. The stability of $Fe_{0.4}$Co-LDH was assessed through chronoamperometric (CA) measurements at an overpotential of 1.459 V **(Figure 3.3h)**.

Table 3.5. The OER activities of ZIF derived electrocatalysts compared with $Fe_{0.4}$Co-LDH@NF.

Sr. No.	Catalyst	Current density (mA cm^{-2})	Overpotential (mV)	Reference
1	**$Fe_{0.4}$Co-LDH@NF**	**20**	**190**	**This work**
2	**ZIF-67@NF**	**20**	**270**	**This work**
3	CoO_x-ZIF	10	318	[32]
4	NiCoP/C nanoboxes	10	330	[33]
5	Co_3O_4@CoP	10	238	[34]
6	Co-P/NC	10	319	[35]
7	Co-P/NC/CC	10	330	[36]
8	Co_3S_4@MoS_2	10	330	[37]
9	M-Co_3O_4/NPC	10	290	[38]
10	Fe-Co_3O_4 HHNPs	10	262	[39]
11	N-Co_3O_4@NC	10	266	[40]
12	Co_3O_4/$NiCo_2O_4$ DSNCs/NF	10	340	[41]
13	Co_3O_4/Co-Fe-oxide DSNBs/GCE	10	297	[42]
14	Co-NC@CoP-NC/GCE	10	330	[43]

$Fe_{0.4}$Co-LDH@NF maintained a stable current density for 40 hours, continuously producing oxygen. After the 40-hour chronoamperometric (CA) measurement, the obtained linear sweep voltammetry (LSV) data was found to be similar to that of the fresh catalyst **(inset, Figure 3.3h)**, confirming the stability of $Fe_{0.4}$Co- LDH@NF. This stability of the catalyst can be attributed to

the strong interaction between the catalyst and NF in a self-supported catalyst system attained by the unique synthesis process.

3.6. Conclusion

Incorporation of Fe(III) in the structure of Co-LDH regulate the local electronic structure, hence increases the electropositivity of the active site Co^{n+}, and facilitates the oxidation and deprotonation of $Co(O)_x(OH)_y$, thereby promoting the formation of Co^{IV} = O species. Consequently, the facile nucleophilic attack of OH^- on Co^{IV} = O leads to the formation of O-O bonds. Remarkably, the strong Lewis acid nature of Fe(III) substantially improves the electronic and electrochemical properties of the active water oxidation catalyst, surpassing the performance of Zn(II) and Co(II), the other two weaker Lewis acids evaluated in this study. The modified electronic structure, improved electrochemical properties, and optimized adsorption of the substrate and reaction intermediates on the catalyst surface result in the "Fe-effect" in the active water oxidation catalyst which resulted in significant improved OER activity.

3.7. References

[1] S. Wang, Q. Jiang, S. Ju, C. S. Hsu, H. M. Chen, D. Zhang, F. Song, *Nat. Commun.* **2022**, *13*, 6650.

[2] B. Singh, A. K. Patel, A. Indra, *Mater. Today Chem.* **2022**, *25*, 100930.

[3] T. Guo, L. Li, Z. Wang, *Adv. Energy Mater.* **2022**, *12*, 2200827.

[4] Y. Wang, D. Yan, S. El Hankari, Y. Zou, S. Wang, *Adv. Sci.* **2018**, *5*, 1800064.

[5] B. Zhang, L. Wang, Z. Cao, S. M. Kozlov, F. P. García de Arquer, C. T. Dinh, J. Li, Z. Wang, X. Zheng, L. Zhang, Y. Wen, O. Voznyy, R. Comin, P. De Luna, T. Regier, W. Bi, E. E. Alp, C. W. Pao, L. Zheng, Y. Hu, Y. Ji, Y. Li, Y. Zhang, L. Cavallo, H. Peng, E. H.

Sargent, *Nat. Catal.* **2020**, *3*, 985.

[6] H. Yang, M. Driess, P. W. Menezes, *Adv. Energy Mater.* **2021**, *11*, 11, 2102074.

[7] A. Karmakar, K. Karthick, S. S. Sankar, S. Kumaravel, R. Madhu, S. Kundu, *J. Mater. Chem. A* **2021**, *9*, 1314.

[8] H. S. Jadhav, H. A. Bandal, S. Ramakrishna, H. Kim, *Adv. Mater.* **2022**, *34*, 2107072.

[9] Y. Wang, J. Cao, Z. Yang, W. Xiong, Z. Xu, P. Song, M. Jia, S. Sun, Y. Zhang, W. Li, *J. Solid State Chem.* **2021**, *294*, 121857.

[10] A. Indra, U. Paik, T. Song, *Angew. Chem., Int. Ed.* **2018**, *57*, 1241.

[11] Z. Chen, Y. Ha, H. Jia, X. Yan, M. Chen, M. Liu, R. Wu, *Adv. Energy Mater.* **2019**, *9*, 1803918.

[12] Y. Lin, H. Wang, C. K. Peng, L. Bu, C. L. Chiang, K. Tian, Y. Zhao, J. Zhao, Y. G. Lin, J. M. Lee, L. Gao, *Small* **2020**, *16*, 2002426.

[13] J. Zhao, X. R. Wang, F. W. Chen, C. He, X. J. Wang, Y. P. Li, R. H. Liu, X. M. Chen, Y. J. Hao, M. Yang, F. T. Li, *Inorg. Chem. Front.* **2020**, *7*, 737.

[14] C. Taviot-Guého, P. Vialat, F. Leroux, F. Razzaghi, H. Perrot, O. Sel, N. D. Jensen, U. G. Nielsen, S. Peulon, E. Elkaim, C. Mousty, *Chem. Mater.* **2016**, *28*, 7793.

[15] N. Iyi, T. Matsumoto, Y. Kaneko, K. Kitamura, *Chem. Mater.* **2004**, *16*, 2926.

[16] B. Singh, A. Yadav, A. Indra, *J. Mater. Chem. A* **2022**, *10*, 3843.

[17] P. Kaspar, D. Sobola, R. Dallaev, S. Ramazanov, A. Nebojsa, S. Rezaee, L. Grmela, *Appl. Surf. Sci.* **2019**, *493*, 673.

[18] Y. Wang, Y. Zhang, Z. Liu, C. Xie, S. Feng, D. Liu, M. Shao, S. Wang, *Angew. Chemie - Int. Ed.* **2017**, *56*, 5867.

[19] A. L. Wang, H. Xu, G. R. Li, *ACS Energy Lett.* **2016**, *1*, 445.

[20] H. Liang, F. Meng, M. Cabán-Acevedo, L. Li, A. Forticaux, L. Xiu, Z. Wang, S. Jin, *Nano Lett.* **2015**, *15*, 1421.

[21] J. Bao, Z. Wang, J. Xie, L. Xu, F. Lei, M. Guan, Y. Zhao, Y. Huang, H. Li, *Chem. Commun.* **2019**, *55*, 3521.

[22] L. Yu, H. Zhou, J. Sun, F. Qin, F. Yu, J. Bao, Y. Yu, S. Chen, Z. Ren, *Energy Environ. Sci.* **2017**, *10*, 1820.

[23] R. Liu, Y. Wang, D. Liu, Y. Zou, S. Wang, *Adv. Mater.* **2017**, *29*, 1701546.

[24] J. Li, W. Xu, R. Li, J. Luo, D. Zhou, S. Li, P. Cheng, D. Yuan, *J. Mater. Sci.* **2016**, *51*, 9287.

[25] A. Guzmán-Vargas, J. Vazquez-Samperio, M. A. Oliver-Tolentino, N. Nava, N. Castillo, M. J. Macías-Hernández, E. Reguera, *J. Mater. Sci.* **2018**, *53*, 4515.

[26] P. Zhou, Y. Wang, C. Xie, C. Chen, H. Liu, R. Chen, J. Huo, S. Wang, *Chem. Commun.* **2017**, *53*, 11778.

[27] J. Han, J. Zhang, T. Wang, Q. Xiong, W. Wang, L. Cao, B. Dong, *ACS Sustain. Chem. Eng.* **2019**, *7*, 13105.

[28] F. Song, X. Hu, *J. Am. Chem. Soc.* **2014**, *136*, 16481.

[29] Y. Liu, M. Zhang, D. Hu, R. Li, K. Hu, K. Yan, *ACS Appl. Energy Mater.* **2019**, *2*, 1162.

[30] B. Singh, P. Mannu, Y. C. Huang, R. Prakash, S. Shen, C. L. Dong, A. Indra, *Angew. Chem., Int. Ed.* **2022**, *61*, e202211585.

[31] S. Anantharaj, S. Kundu, S. Noda, *Nano Energy* **2021**, *80*, 105514.

[32] S. Dou, C. L. Dong, Z. Hu, Y. C. Huang, J. L. Chen, L. Tao, D. Yan, D. Chen, S. Shen, S. Chou, S. Wang, *Adv. Funct. Mater.* **2017**, *27*, 1702546.

[33] P. He, X. Y. Yu, X. W. D. Lou, *Angew. Chem., Int. Ed.* **2017**, *56*, 3897.

[34] J. Zhou, Y. Dou, A. Zhou, R. M. Guo, M. J. Zhao, J. R. Li, *Adv. Energy Mater.* **2017**, *7*, 1602643.

[35] B. You, N. Jiang, M. Sheng, S. Gul, J. Yano, Y. Sun, *Chem. Mater.* **2015**, *27*, 7636.

[36] X. Liu, J. Dong, B. You, Y. Sun, *RSC Adv.* **2016**, *6*, 73336.

[37] Y. Guo, J. Tang, H. Qian, Z. Wang, Y. Yamauchi, *Chem. Mater.* **2017**, *29*, 5566.

[38] X. Yang, J. Chen, Y. Chen, P. Feng, H. Lai, J. Li, X. Luo, *Nano-Micro Lett.* **2018**, *10*, 15.

[39] S. L. Zhang, B. Y. Guan, X. F. Lu, S. Xi, Y. Du, X. W. Lou, *Adv. Mater.* **2020**, *32*, 2002235.

[40] Z. Wang, W. Xu, X. Chen, Y. Peng, Y. Song, C. Lv, H. Liu, J. Sun, D. Yuan, X. Li, X. Guo, D. Yang, L. Zhang, *Adv. Funct. Mater.* **2019**, *29*, 1902875 .

[41] H. Hu, B. Guan, B. Xia, X. W. Lou, *J. Am. Chem. Soc.* **2015**, *137*, 5590.

[42] X. Wang, L. Yu, B. Y. Guan, S. Song, X. W. (David) Lou, *Adv. Mater.* **2018**, *30*, 1801211.

[43] X. Li, Q. Jiang, S. Dou, L. Deng, J. Huo, S. Wang, *J. Mater. Chem. A* **2016**, *4*, 15836.

[44] C. C. L. McCrory, S. Jung, J. C. Peters, T. F. Jaramillo, *J. Am. Chem. Soc.* **2013**, *135*, 16977.

[45] S. Anantharaj, S. Kundu, *ACS Energy Lett.* **2019**, *4*, 1260.

[46] S. Anantharaj, S. R. Ede, K. Karthick, S. Sam Sankar, K. Sangeetha, P. E. Karthik, S. Kundu, *Energy Environ. Sci.* **2018**, *11*, 744.